National Laser Users' Facility News

During FY01, 600 OMEGA target shots were taken for external users. This is a 5.1% increase over FY00 and the highest number of target shots ever taken by OMEGA external users in a single year, accounting for ~47% of the total 1289 target shots taken on the system. The external users included eight collaborative teams carrying out work under the National Laser Users' Facility (NLUF) Program as well as collaborations led by scientists from Lawrence Livermore National Laboratory (LLNL), Los Alamos National Laboratory (LANL), Sandia National Laboratory (SNL), the Nuclear Weapons Effects Testing (NWET) Program, and Commissariat à l'Énergie Atomique (CEA) of France.

FY01–FY02 NLUF Experiments

FY01 was the first year that NLUF programs were approved for a two-year period of performance (FY01 and FY02). The eight NLUF experimental campaigns received a total of 125 OMEGA target shots in FY01.

The independent DOE Technical Evaluation Panel for this period, consisting of Dr. David Bradley (LLNL), Dr. David Montgomery (LANL), Dr. Richard Olson (SNL), and Dr. Ned Sauthoff (Princeton Plasma Physics Laboratory), reviewed progress reports submitted in September 2001 by all of the current participants, confirmed that all eight participants made satisfactory progress during FY01, and recommended continued funding and shot allocations for all of the programs through FY02.

In 2Q02 DOE is expected to issue a new solicitation for NLUF programs to be carried out during FY03–FY04. The NLUF shot allocation for FY03 is 12 OMEGA shot days (~120 target shots). The NLUF DOE funding allocation for FY01 and FY02 was $700,000 to cover the participants' costs for carrying out experiments on OMEGA. It is expected that this funding level may increase in FY03/FY04 to a level more consistent with the high level of interest shown in the use of OMEGA to carry out high-energy-density physics experiments of relevance to the National Nuclear Security Agency (NNSA) Stockpile Stewardship Program (SSP).

The eight NLUF experimental campaigns carried out in FY01 included the following:

Atomic Physics of Hot, Ultradense Plasmas.
Principal Investigators: C. F. Hooper Jr. (University of Florida), D. A. Haynes (Fusion Technology Institute, University of Wisconsin), and collaborators from Los Alamos National Laboratory, the University of Wisconsin, and LLE.

The plasma environment perturbs atomic processes of radiators immersed in hot, dense plasmas. This perturbation is a challenging application of the statistical mechanics of dense plasmas and leads to observable and diagnostically useful variations in the spectrum emitted by the radiators. The focus of this work is to produce hot [electron temperature (T_e) > 1.5 keV], ultradense [electron density (n_e) ~ 5×10^{24} cm^{-3}] plasmas using the OMEGA laser in direct-drive mode. In FY01 eleven shots were performed toward this objective. Ar-doped (1% to 2% by atom) CH shells (940-μm diameter, 20 μm thick) filled with 15 atm of deuterium were used in these experiments. With 23-kJ-energy, 1-ns square laser pulses, a core $n_e > 2 \times 10^{24}$ cm^{-3} and T_e ~ 1.15 keV were observed. Because simulations indicated that ramped pulse shapes can achieve electron densities in the range of 5×10^{24} cm^{-3} to 8×10^{24} cm^{-3}, a series of ramped pulse shots were taken later in the year. These data are currently being analyzed.

Determination of Temperature and Density Gradients in Implosion Cores of OMEGA Targets.
Principal Investigators: R. C. Mancini (University of Nevada, Reno), J. A. Koch (LLNL), and collaborators from the University of Wisconsin, LLE, LLNL, and Howard University.
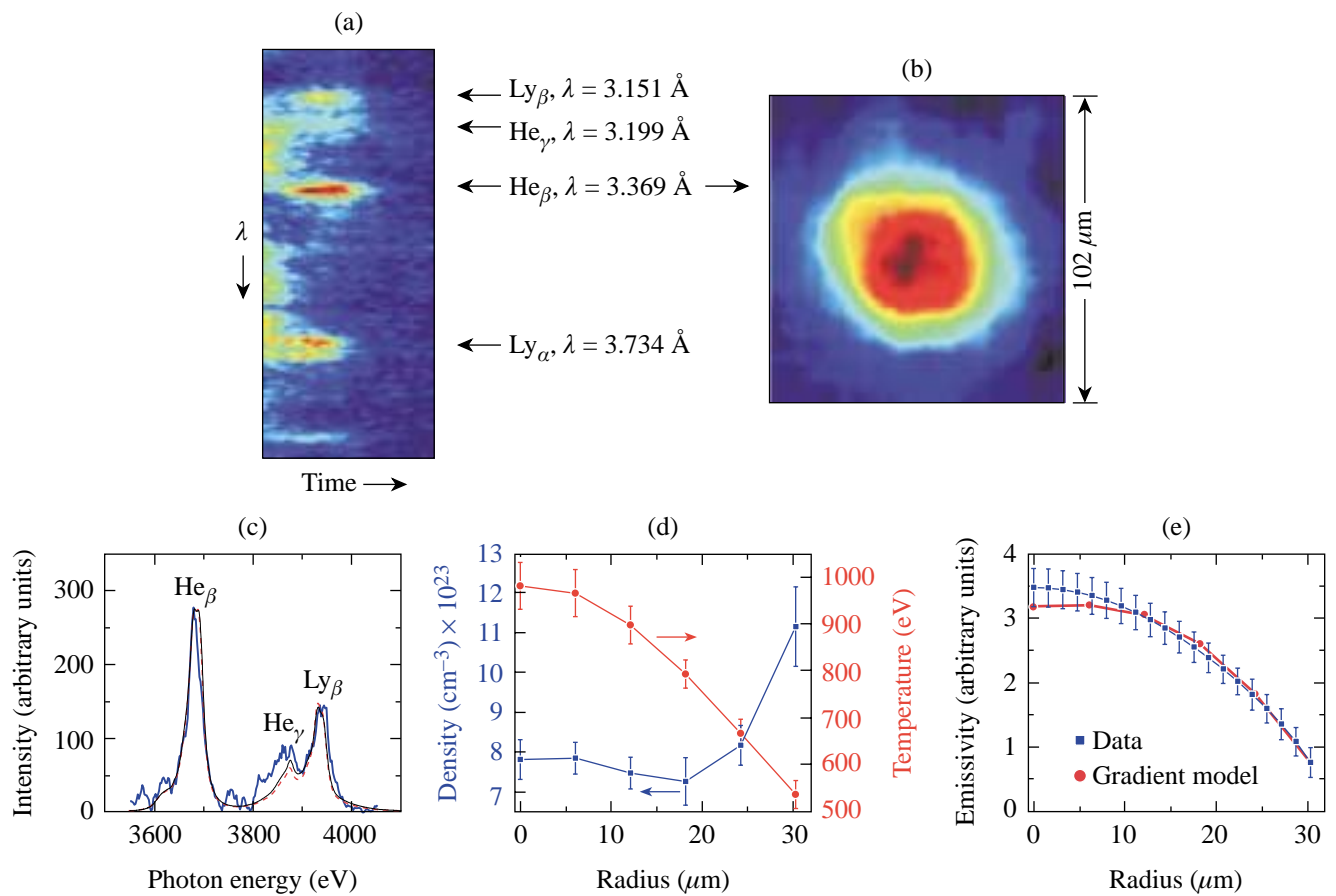
The goal of this project is to determine time-resolved temperature and density gradients in implosion cores on OMEGA indirect-drive implosion experiments using x-ray spectroscopy. The method is based on a novel self-consistent analysis of data from simultaneous, time-resolved x-ray line spectra and x-ray monochromatic images. Argon-doped, deuterium-filled plastic shells placed in gold hohlraums and driven

by 30 UV laser beams of OMEGA were used in these experiments. The aim was to achieve stable, spherically symmetric, and reproducible implosion cores where the proposed spectroscopic gradient determination technique can be tested and established. During FY01, a target design was successfully tested, and argon *K*-shell x-ray line spectra and monochromatic images were recorded on several shots (see Fig. 88.43).

Studies of Fundamental Properties of High-Energy-Density Plasmas.
Principal Investigator: R. Petrasso (MIT Plasma Science and Fusion Center) and collaborators from LLE, LLNL, and SUNY Geneseo.

In FY01, four different types of experiments were carried out under this program. In the first experiment, slowing-down measurements of nascent 14.7-MeV protons generated by D^3He fusion reactions were made in up to eight different directions on the same target shot to characterize the capsule's total ρR variations (see Fig. 88.44). These measurements were carried out using compact wedged range filters (WRF's). In the second class of experiments, DTH-filled CD capsules were imploded with the aim of using knock-on protons to determine the fuel ρR. In the third series of experiments, fuel–shell mix was studied by determining how much shell material is combined with the fuel at burn time. In the final set of experiments, the total ρR's at the times of shock coalescence and stagnation


(a)

← Ly_β, λ = 3.151 Å
← He_γ, λ = 3.199 Å

← He_β, λ = 3.369 Å →

← Ly_α, λ = 3.734 Å

λ ↓

Time →

(b)

102 μm

(c)

(d)

(e)

U264

Figure 88.43
(a) Time-resolved argon *K*-shell x-ray spectrum and (b) time-integrated He_β line monochromatic image from the implosion core of OMEGA shot 23686. (c) Synthetic spectra fits to the x-ray spectrum time-integrated over the emission interval of the He_β line; the red dashed line is the gradient model, the thin blue line is the uniform model, and the thick blue line is the experimentally measured spectrum. (d) Electron temperature and number density core gradients. (e) Synthetic emissivity fit to the He_β emissivity profile extracted from the monochromatic image. The emissivity-weighted averages of the gradients, $\langle N_e \rangle_\varepsilon = 7.8 \times 10^{23}$ cm^{-3} and $\langle T_e \rangle_\varepsilon = 860$ eV, show good consistency with the results of the uniform model analysis.

were differentiated. This measurement is based on a comparison of the measured energy spectra of the D^{3}He primary protons in implosions of D^{3}He-filled CH shells to those of CD/CH shells filled with only ^{3}He (see Fig. 88.45).
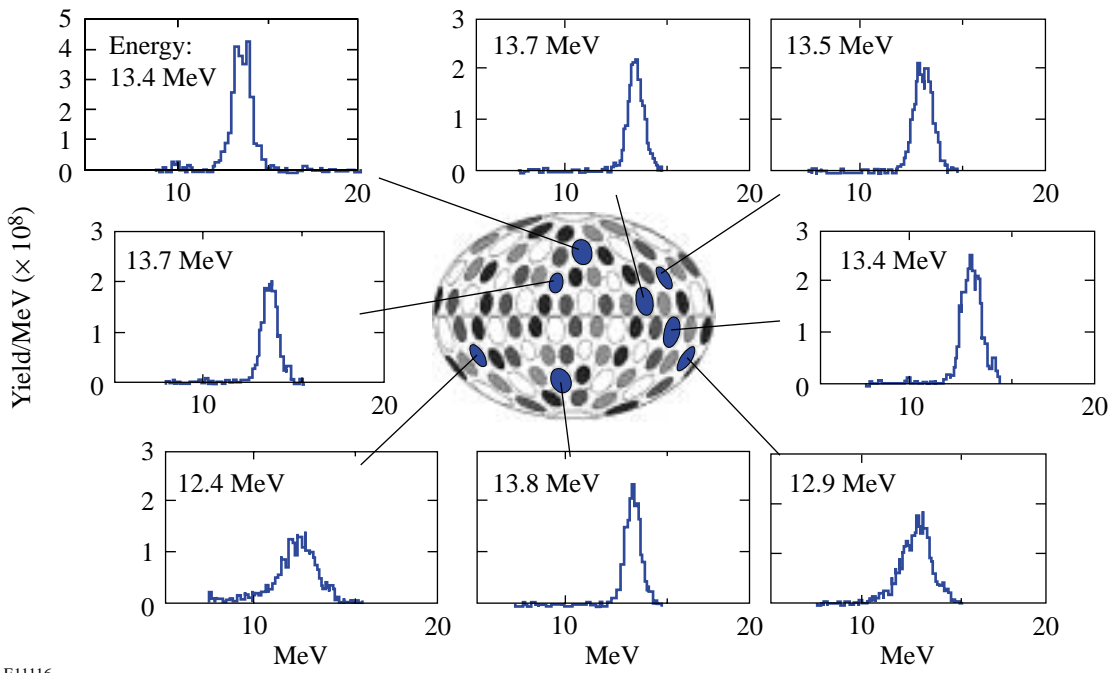
Figure 88.44

Data showing 14.7-MeV primary proton slowing down from the implosion of a D^{3}He-filled capsule. These data are obtained by a combination of seven wedged-range filters (WRF's) and two charged-particle spectrometers (CPS's). Note the variation in mean energy of the protons as a function of angular position. These data imply that there are significant low-ℓ-mode variations in the total areal density of the imploded capsule.
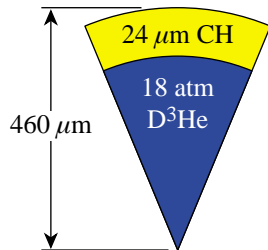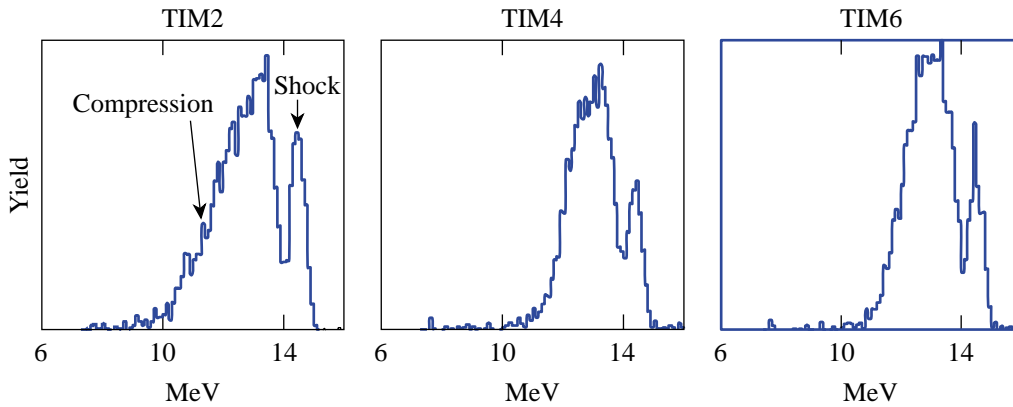

Figure 88.45

WRF data from OMEGA shot 24811 showing primary proton spectra from three different directions. The proton yield at shock time and that produced at peak compression are distinguished by the difference in mean proton energy. The protons generated at the time of the first shock have only a small downshift in energy (~0.3 MeV) corresponding to the lower capsule areal density expected at shock time (~8 mg/cm^2) compared to a downshift of ~2.3 MeV at peak compression corresponding to a ρR ~ 70 mg/cm^2.

Studies of the Dynamic Properties of Shock-Compressed FCC Crystals by In-Situ *Dynamic X-Ray Diffraction.*
Principal Investigators: H. Baldis (University of California at Davis), D. H. Kalantar (LLNL), and collaborators from LLNL, LLE, University of California at San Diego, University of Oxford, and LANL.

This experiment uses time-resolved dynamic x-ray diffraction to study the response of a lattice under shock compression as the shock passes through the sample. Recovery of target samples for laboratory examination allowed the residual deformation effects to be examined directly. The shots this year were aimed at developing the capability to record diffraction from multiple lattice planes during passage of a shock through a thin foil of single-crystal copper. Simultaneous recovery of separate shock samples experiments were conducted.

During FY01, the diffraction from the (200) and (020) lattice planes of Cu were recorded using a V x-ray source (2.38 Å). In addition, a modified target was tested using a Cu x-ray source (1.4 Å) to record the (400) lattice planes of Cu. Fielding a large-solid-angle film holder on diffraction experiments taken in August 2001 extended the technique further (see Fig. 88.46).

High-Spatial-Resolution Neutron Imaging of Inertial Fusion Target Plasmas Using Bubble Neutron Detectors.
Principal Investigator: Raymond K. Fisher (General Atomics) and collaborators from LLE, CEA, and LLNL.

Bubble detectors capable of detecting neutrons with a spatial resolution of 5 to 30 μm are one of the most-promising approaches to imaging NIF target plasmas with the desired 5-μm spatial resolution in the target plane. Gel bubble detectors are being tested to record neutron images of ICF implosions in OMEGA experiments. By improving the noise reduction techniques used to analyze the data taken in June 2000, it was possible to image the neutron emission from 6×10^{13}-yield DT target plasmas with a target plane spatial resolution of ~140 μm, as shown in Fig. 88.47. As expected, the spatial resolution was limited by counting statistics as a result of the low neutron detection efficiency of the easy-to-use gel bubble detectors. The results, which have been submitted for publication, were presented as an invited talk at the October 2001 Meeting of the Division of Plasma Physics of the American Physical Society.

To improve the counting statistics, data taken in May 2001 using a stack of four gel detectors were integrated over a series
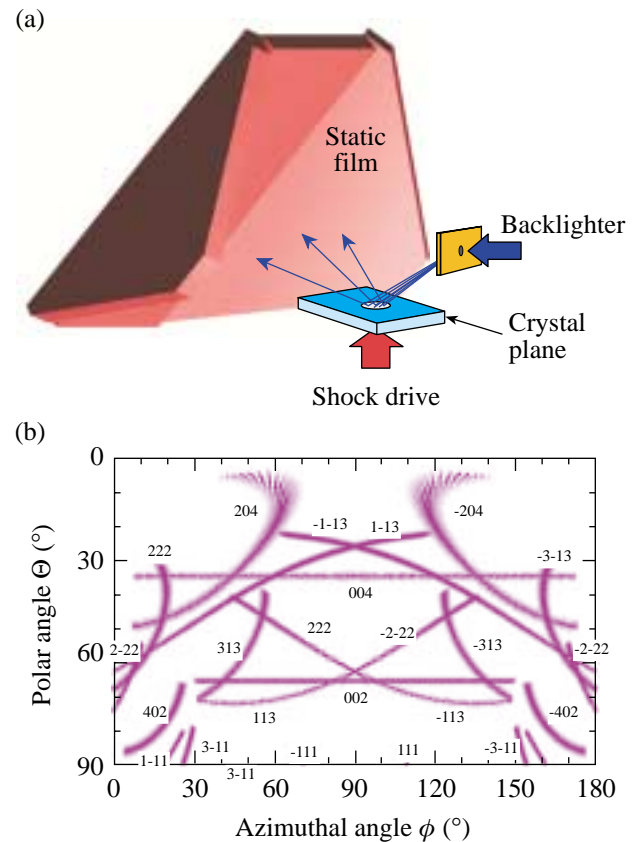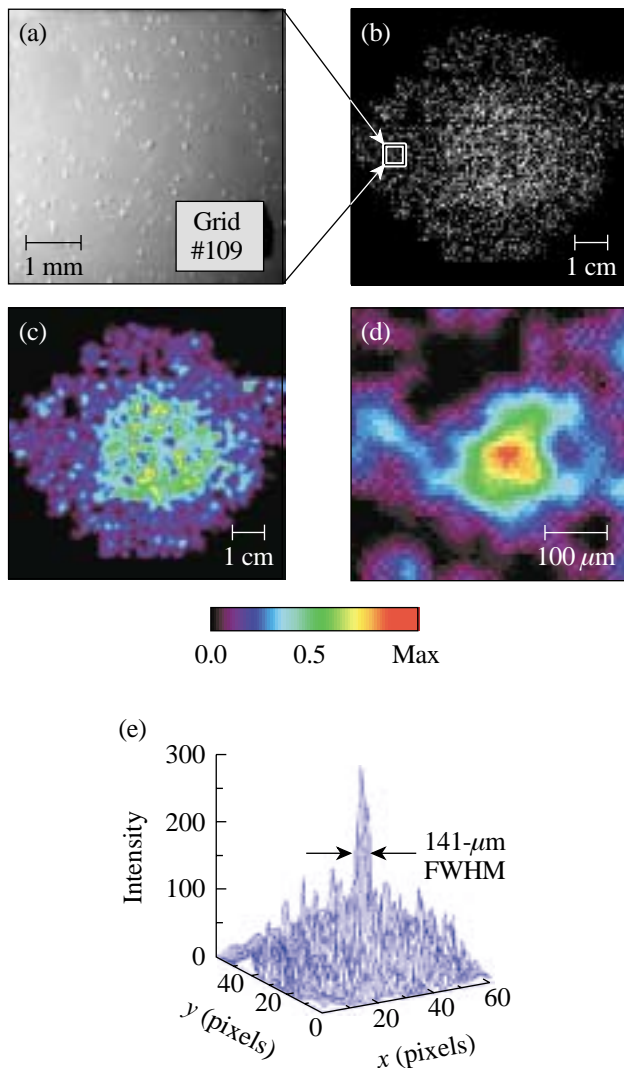

Figure 88.46
(a) Schematic of a static film-based detector that records x rays diffracted from many different lattice planes covering nearly a π-steradian solid angle.
(b) Simulated diffraction pattern from multiple lattice planes of Si.

of up to seven high-yield DT shots. Analysis of the 2001 data is still in its early stages. Gel detectors were chosen for these initial tests since the bubbles can be photographed several hours after the neutron exposure. They consist of ~5000 drops (~100 μm in diameter) of bubble detector liquid/cm^3 suspended in an inactive support gel that occupies ~99% of the detector volume. Using a liquid bubble chamber detector, along with a light-scattering system to record the bubble locations a few microseconds after the neutron exposure when the bubbles are ~10 μm in diameter, should result in ~1000 times higher neutron detection efficiency and a target plane resolution on OMEGA of ~10 to 50 μm.

Examination of the "Cone-in-Shell" Target Compression Concept for Asymmetric Fast Ignition.
Principal Investigators: Richard B. Stephens (General Atomics) and collaborators from LLNL and the Institute of Laser Engineering (ILE), Osaka University, Osaka, Japan.

(a)

Grid #109

1 mm

(b)

1 cm

(c)

1 cm

(d)

100 μm

0.0   0.5   Max

(e)

U266

Figure 88.47

Bubble detector images from a 6×10^{13}-yield OMEGA shot, including (a) a microscope photograph of 60-μm-diam bubbles in a single grid location, (b) an x–y plot of bubble locations, (c) a coded false color image in the detector plane, and (d) and (e) an unfolded neutron image in the target plane.

Studies of the compression hydrodynamics of targets suitable for the fast-ignition inertial fusion concept have been initiated. The objective is to assemble a dense core of material while maintaining clear access for the ignition pulse through the low-density blowoff. A hollow, high-density cone inserted in the side of the shell and placed inside a cylindrical hohlraum can be used to maintain the ignition pulse access. The cone causes anisotropies in the shell implosion: radiation intensity changes and shear near the cone surface modify the local implosion velocity, and the dense core is assembled from only a partial shell. Modeling (Steve Hatchett, LLNL) suggested

that the consequences of these asymmetries would be relatively minor; it should be feasible to assemble a dense, nearly spherical core with a piece missing. A model system using a hohlraum-driven target was set up to test prediction, and backlit framing camera pictures of the model system were compared to the simulation. The predicted and experimental images look similar (see Fig. 88.48) but there were subtle differences. The collapse time might have changed since the experimental shell density was about half that expected in the interval of the framed images. In addition, the shell seems less separated from the cone, and the cone shape is less defined in the experimental images compared to the simulation. Further analysis will continue in order to understand these changes and to optimize our experimental setup for the next round of experiments.

Supernova Hydrodynamics on the OMEGA Laser.
Principal Investigators: R. Paul Drake (University of Michigan), B. Remington (Center for Laser Astrophysics-ILSA, LLNL), and collaborators from LLNL, CEA Saclay (France), LLE, LANL, University of Arizona, University of Colorado, University of Chicago, SUNY Stony Brook, Naval Research Laboratory, and Eastern Michigan University.

The fundamental motivation of this program is that supernovae are not well understood. Experiments are performed in compressible hydrodynamics and radiation hydrodynamics, relevant to supernovae and supernovae remnants. These experiments produce phenomena in the laboratory that are thought, based on simulations, to be important to astrophysics but that have not been directly observed either in the laboratory or in an astrophysical system. During FY01, this work has focused on the production of an astrophysically relevant, radiative shock and on the three-dimensional, deeply nonlinear evolution of the Rayleigh–Taylor (RT) instability at a decelerating, embedded interface. These experiments required strong compression and decompression, strong shocks (Mach ~ 10 or greater), flexible geometries, and very smooth laser beams, which means that the 60-beam OMEGA laser is the only facility capable of carrying out this program.

Highlights of these Supernova Hydrodynamics experiments include the following:

a. Radiative Precursor Shocks: These experiments involved the initial acceleration of a block of material to high velocity with up to ten OMEGA beams. This block of material then drove a shock wave through low-density foam at a velocity of ~100 km/s, which was fast enough to produce a radiative
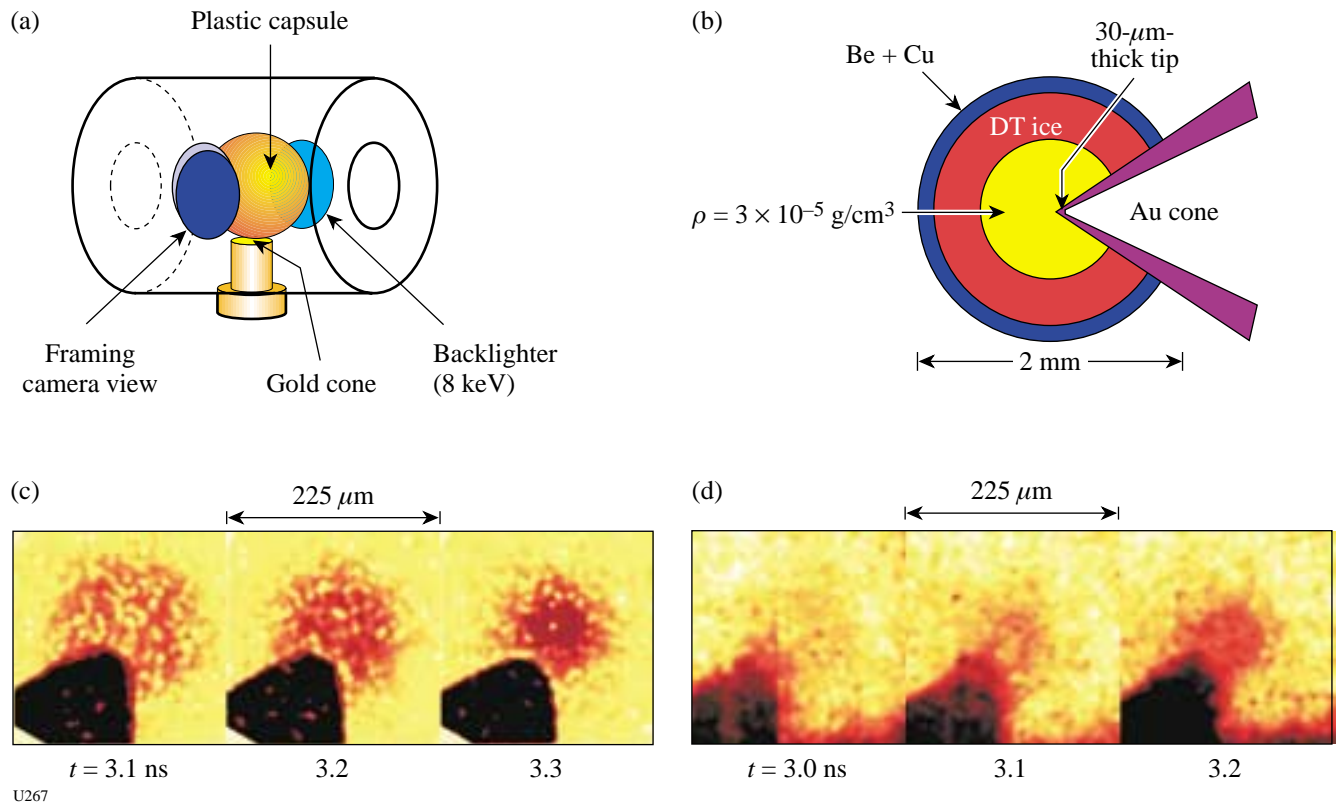
Figure 88.48
(a) Schematic of NIF-scale fast-ignition target; (b) schematic of OMEGA-scale experiment to test the concept; (c) computer simulation of x-ray backlit images of an OMEGA target; and (d) observed backlit images of an OMEGA target experiment just before stagnation.

precursor. The structure of the precursor was diagnosed with absorption spectroscopy using a thulium target. Absorption lines were detected from up to six different ionization states (see Fig. 88.49). The lines from higher ionization states appear at higher temperatures. This allows one, with the help of the OPAL atomic code,[1] to determine the temperature profile in the precursor. It is expected that such experiments will provide quality benchmark cases for astrophysical modeling.

b. 2-D versus 3-D Rayleigh–Taylor: A major issue in the evolution of supernovae is whether three-dimensional effects can resolve the differences between reality and simulations, nearly all of which are carried out in two dimensions. A few 3-D simulations, not yet benchmarked, suggest that 3-D effects are not sufficient to resolve these differences. During FY01, experiments were continued to compare the deep nonlinear evolution of the RT instability at an embedded interface in both two dimensions and three dimensions (examples from two FY00 shots are shown in Fig. 88.50).

c. Multimode Perturbations and the Onset of Turbulence: During the past year, the study of RT at an embedded interface was extended to begin to examine the growth of multimode perturbations. In addition, the experimental system was analyzed in the context of recent theories regarding the onset of turbulence at shear layers like those between the bubbles and the spikes.

d. Spherically Diverging Experiments: During the past year, a small amount of improved data was obtained on spherically diverging unstable systems. Papers now in progress describe the results obtained on these experiments.
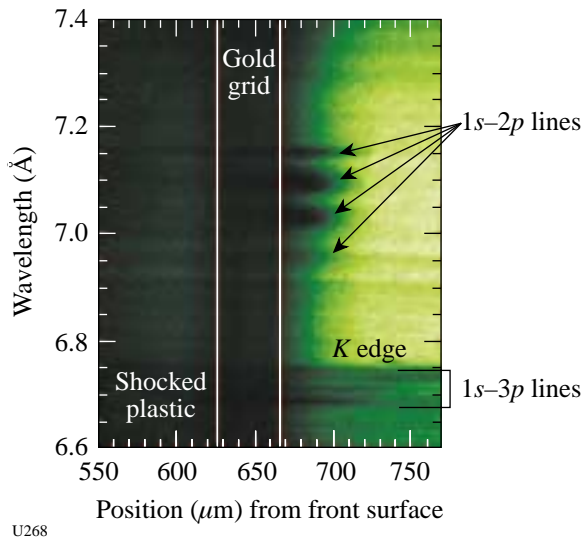
Figure 88.49
An absorption spectrum from the radiative precursor shock experiments at 5.5 ns after the onset of a 1-ns laser pulse The absorption lines extending to the right of the grid in the image can be analyzed to determine the temperature profile. Initial results show a much shorter precursor than simulations predict.

Optical-Mixing-Controlled Stimulated Scattering Instability Experiments on OMEGA (III) and (IV): Suppressing Backscattering Instabilities by the Externally Controlled Generation of Ion-Acoustic Turbulence.
Principal Investigator: Bedros Afeyan (Polymath Research Inc.) and collaborators from LANL, University of Nevada at Reno, LLNL, and LLE.

The prime objective of this program is to suppress backscattering instabilities by the externally controlled generation of ion-acoustic-wave (IAW) and electron-plasma-wave (EPW) turbulence in different IAW damping regimes. During FY01, the work was directed toward two goals: (1) to generate large-amplitude IAW's at or near the Mach-1 surface of an exploding-foil target (on the pump side of the density peak), and (2) to measure how this reduces the stimulated Raman scattering (SRS) and stimulated Brillouin scattering (SBS) backscattering levels of the pump when the probe/pump energy ratio is high enough.

Planar-foil targets of 5-μm-thick Be were used for the first time this year. According to the hydrodynamic simulations, these Be targets are hydrodynamically similar to the 10-μm-CH targets used in previous years' experiments. A major result of this year's work was the demonstration for the first time in
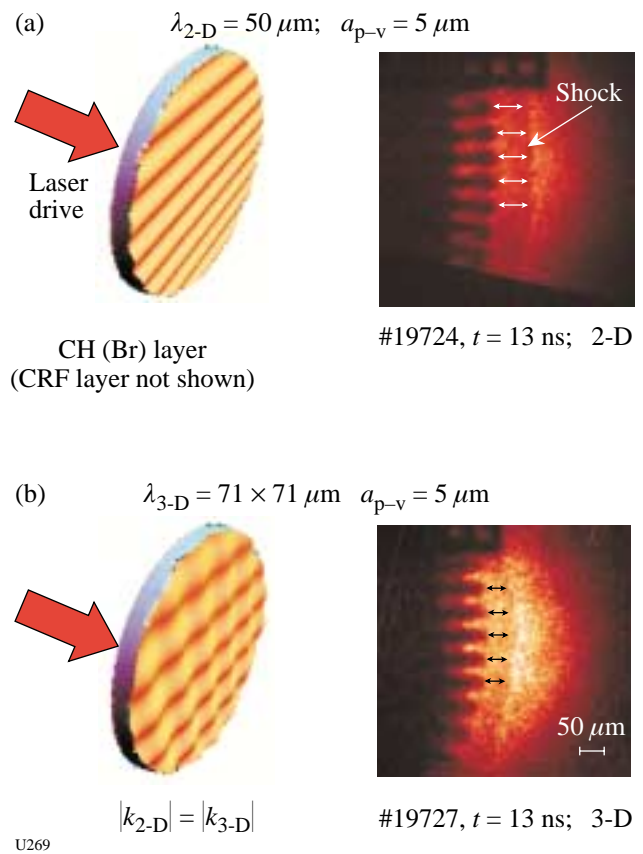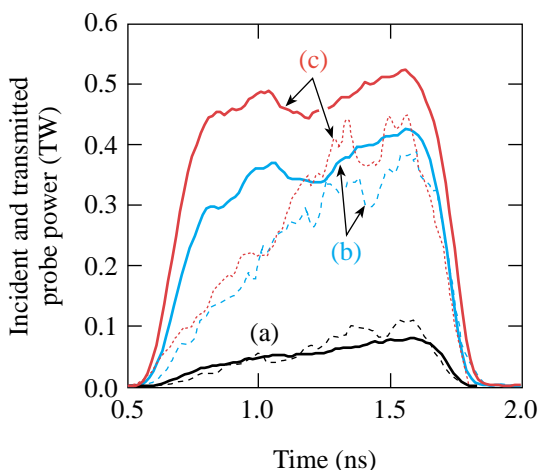

Figure 88.50
Spikes produced by the Rayleigh–Taylor instability during the deceleration of a structured interface. The spikes produced by a 3-D "egg crate" pattern (b) are longer and extend closer to the shock than those produced by a rippled (2-D) interface (a).

equal-frequency crossed beam experiments in flowing plasmas of greater-than-100% transmission of a probe beam intensity due to its interaction with the pump beam and the subsequent energy transfer (see Fig. 88.51). It was also shown that SRS backscattering of the pump beam is suppressed by a factor of 6 or more in the presence of a large IAW driven by the crossing pump and probe beams at or near the Mach-1 surface even in this weak IAW damping limit.

The quality of this year's experiments was improved because it was possible to carry out probe beam intensity scaling experiments using "frequency-conversion-crystal detuning" to adjust the probe beam amplitude. This technique, attempted for the first time during these OMC SSI experiments, allows nearly square, 1-ns laser pulses to be generated over the UV energy range of 30 J to 500 J on target without adjusting the input laser pulse shape of the OMEGA laser.

U270

	Incident probe energy (J)	Energy transfer (%)
a	61	109
b	378	68
c	510	58

FY01 National Laboratory, NWET, and CEA Programs

OMEGA continued a high rate of shot production for external users from the national laboratories (LLNL, LANL, and SNL) as well as from the Nuclear Weapons Effects Testing (NWET) Program, the United Kingdom Atomic Weapons Establishment (AWE), and the Commissariat à l'Énergie Atomique (CEA) of France. A total of 475 target shots were taken for these programs in FY01. The following is a brief summary:

1. LLNL and NWET Campaigns

In FY01 LLNL had 320 shot opportunities at the OMEGA facility, divided as follows: 110 shots for target ignition physics (TIP), 190 shots for high-energy density science (HEDS), and 20 shots for NWET. These opportunities resulted in 312 actual target shots, involving 19 principal investigators (including several shots with collaborators from SNL and LANL). The mini-campaigns are listed in Table 88.XI.

Highlights of LLNL and NWET experiments in FY01 include the following:

Laser–Plasma Interactions: Energy transfer between beams was observed in the forward-scatter geometry and for a range of beam and plasma conditions that are similar to those expected in the NIF. In some cases, the beam energy was enhanced by as much as a factor of 2. This has the potential for creating a symmetry problem for NIF indirect-drive capsules. Substantial energy transfer was observed even at 1/5 the nominal NIF intensity. This indicates that large beams alone may not solve the symmetry problem for indirect-drive capsules. The OMEGA data will motivate an investigation of the energy transfer issue for a variety of possible NIF target/beam configurations in order to select the optimum configuration.
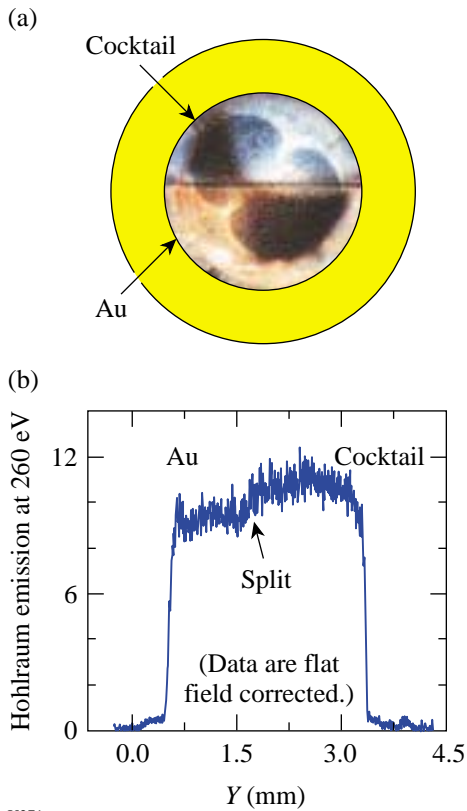
Cocktail Hohlraums: Experiments to investigate the potential of "cocktail" hohlraum materials to increase soft x-ray emission (and therefore increase the energy coupling to the capsule) in NIF hohlraums were continued. In FY01, Scale 3 hohlraums with a splitback plate (see Fig. 88.52) indicated that the soft x-ray emission of the cocktail material at a photon energy of 260 eV is only 15% enhanced over the case of a conventional hohlraum made only of Au (see Fig. 88.52). In addition, Scale 3/4 and Scale 1 cocktail hohlraums gave the same spectrally integrated drive as gold hohlraums, whereas a 5% increase in T_r was expected. This unexpected observation may be due to lower laser to x-ray conversion efficiency for cocktail hohlraums compared to the standard Au hohlraums. A potential fix to be tested in FY02 is to use Au-lined cocktail hohlraums such that the laser conversion to x rays still occurs in the top Au layer, while the reradiation energetics is dominated by the deeper cocktail layer.

High-Convergence Implosions: The multicone capability of OMEGA continued to be of use in conducting cylindrical-hohlraum capsule implosions with convergence ratios as high as 20. In FY01 HEP5 experiments, the improvement in performance over Nova experiments with similar targets was ascribed to better time-dependent symmetry control and the use of Ar dopant-free fuel (see Fig. 88.53). Experiments with intentionally roughened surfaces demonstrated that the degradation was caused by hydro-instability growth and followed simulation results (see Fig. 88.54).

Table 88.XI: FY01 LLNL and NWET Campaigns.

Campaign	Sub-Element	Experiment	Target Shot Allocation
Target Ignition Physics (TIP)	WBS-1: Energetics	Absolute albedo	5
		Laser–plasma interactions	10
		Cocktail holhraum	10
	WBS 2: Symmetry	NIF foot symmetry	10
		High-convergence implosions	20
	WBS 3: Ablator Physics	Shock timing	20
		Ablator burnthrough	5
		Convergent ablator burnthrough	10
		Planar RT	10
		X-ray Thomson scattering	5
	WBS 4: Diagnostics	Ignition diagnostics	5
High-Energy-Density Sciences		Solid-State Hydro	20
	Implosion Mix	Pushered shells	10
	Hydro I	Richtmyer–Meshkov	20
	Hydro II	Features	15
	Hydro III	Jets	15
	Implosions	NBI	5
	Radiation Transport	RadG	20
	Equation of State (EOS)	Low- and High-Z	35
		X-ray Thomson scattering	5
	Opacity	Hot holhraum	10
		NLTE	5
	Capability Development	X-ray Thomson scattering	10
		Backlighter development	5
		Slit closure	5
		Dual color	10
NWET	Source Development	Gas-filled sources	10
		Hot-electron sources	5
		Spheres	5
		TOTAL	320

(a)

Cocktail

Au

(b)

NIF-Relevant Hohlraum Symmetry: Investigation of the symmetry of NIF-relevant (WBS 2) hohlraums continued. A configuration for these experiments is shown in Fig. 88.55(a). Thin-shell implosions were imaged with 4.7-keV x rays and yielded symmetry data showing that the asymmetries are small and in agreement with 2-D simulations [see Fig. 88.55(b)].
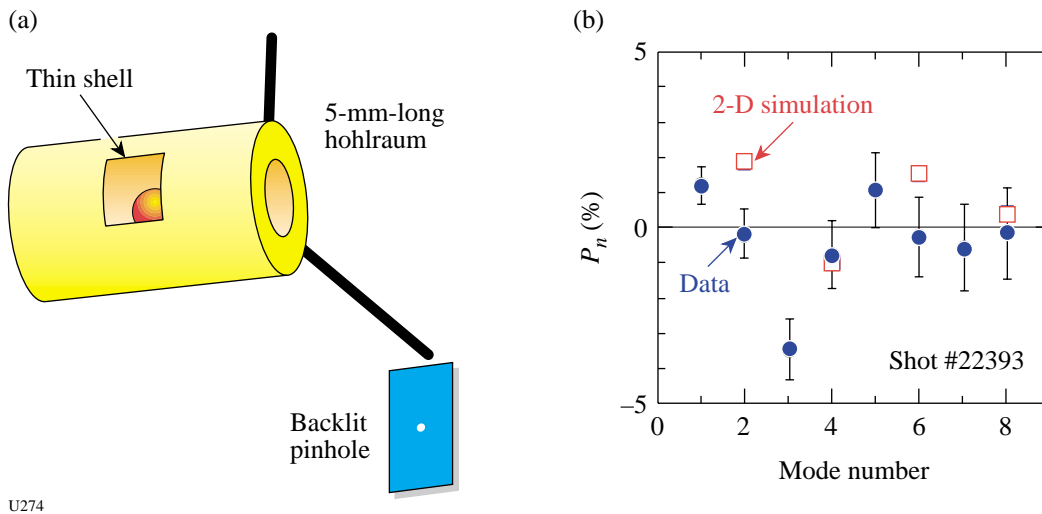
Figure 88.52

(a) Schematic of the hohlraum configuration used to conduct cocktail material experiments. A split backplate (half cocktail/half Au) is used in a Scale 3 hohlraum. (b) Soft x-ray emission at 260 eV is spatially resolved and shows an ~15% increase in cocktail soft x-ray emission compared to the Au side. This increase is lower than that predicted by *LASNEX* simulations.
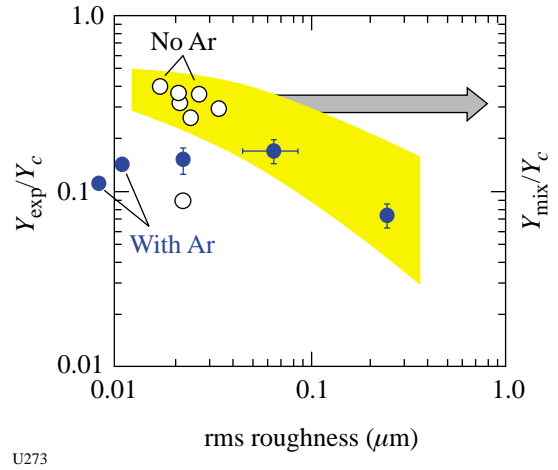
Figure 88.54

Plot of the ratio of measured neutron yield over that calculated for 1-D clean implosions as a function of measured target roughness. The cases shown are for convergence ratio ~ 20, indirect-drive implosions carried out on OMEGA. The capsules were intentionally roughened to carry out this experiment. The results are compared to simulations (yellow band) showing the ratio of the neutron yield for an implosion with mix to that of clean 1-D implosions.
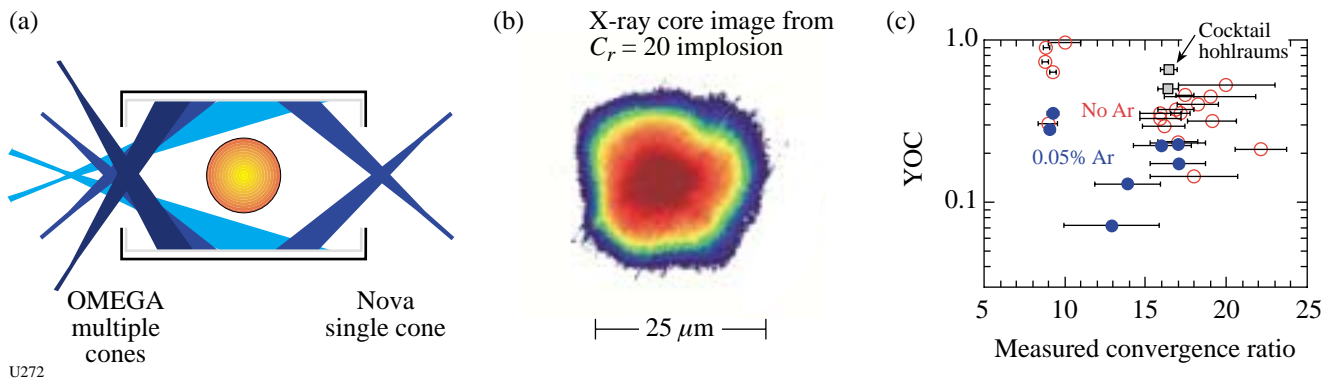
Figure 88.53

(a) Schematic showing the difference between the Nova single-cone hohlraum geometry and that of OMEGA with multiple cones. (b) Typical x-ray image of OMEGA implosion shows symmetric implosion for capsules with convergence ratio ~ 20. (c) Plot of the ratio of actual neutron yield divided by the calculated 1-D clean yield (YOC) as a function of measured convergence ratio. The improvement in performance of the OMEGA experiments (open circles) over Nova implosions (solid circles) is ascribed to better time-dependent symmetry control and the use of dopant-free fuel.
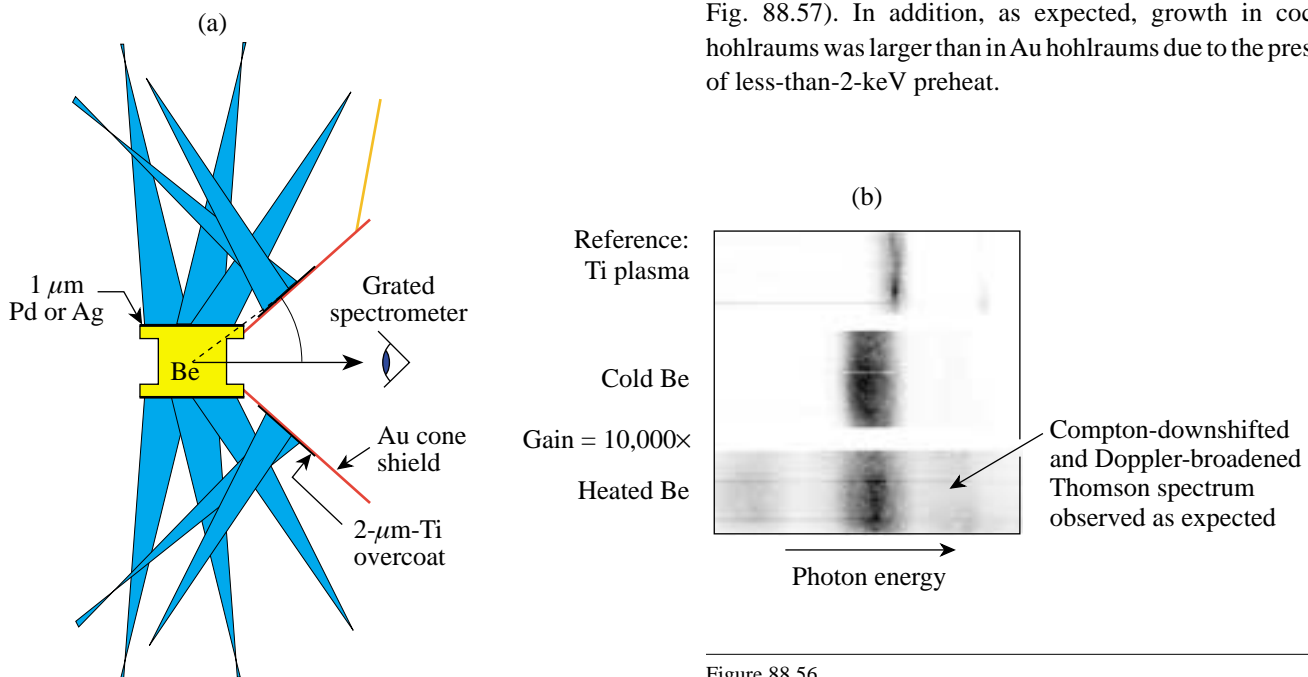
Figure 88.55
Schematic of experimental geometry for OMEGA symmetry experiments. A thin spherical target is imploded inside a 5-mm-long cylindrical hohlraum (a). A point source backlighter provides high-resolution x-ray radiographic images. The resulting data are plotted in (b) showing the inferred asymmetries decomposed in Legendre moments P_n. The open square data points are the results of a 2-D simulation of the asymmetry while the solid circles are the experimental results.

X-Ray Thomson Scattering: The first demonstration of x-ray Thomson scattering as a high-density temperature and density diagnostic was carried out on OMEGA during FY01. The experimental configuration is shown in Fig. 88.56(a). Initial results from these experiments are shown in Fig. 88.56(b).

Planar Rayleigh–Taylor Experiments: Polyimide ablator Rayleigh–Taylor (PIRT) experiments continued on radiation-driven targets in FY01. Experiments conducted with 30-, 50-, and 70-μm-wavelength perturbations showed that the RT growth rate with small initial amplitudes was somewhat greater than originally predicted and occurred somewhat earlier (see Fig. 88.57). In addition, as expected, growth in cocktail hohlraums was larger than in Au hohlraums due to the presence of less-than-2-keV preheat.

Figure 88.56
(a) Schematic of x-ray Thomson scattering experiment. (b) Experimental results from x-ray Thomson scattering experiment.
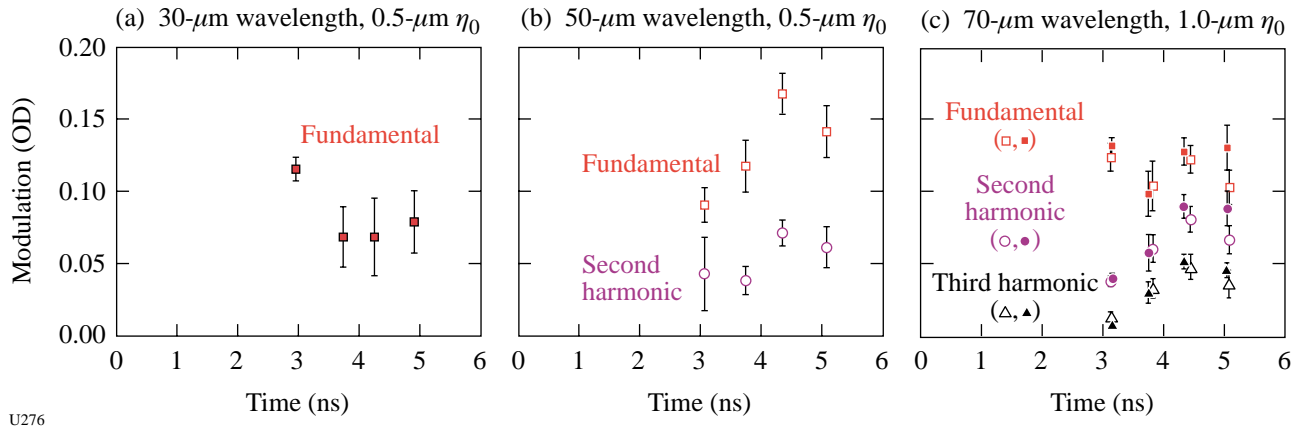
Figure 88.57
Summary of RT growth data from PIRT experiments with Au (open data points) and cocktail (solid points) hohlraums. More growth is evident in cocktail hohlraums than in Au hohlraums. Future shots will attempt to reproduce these results and expand the database.

Shock Timing: A collaboration including scientists from SNL, LANL, and LLNL conducted experiments to investigate shock timing in radiation-driven ablators. A half-hohlraum (halfraum) target was used for these experiments. One configuration featured stepped or wedged ablators attached to a halfraum and interrogated with a LANL streaked optical pyrometer (SOP) as shown in Fig. 88.58. Experiments were also conducted using flat ablator samples and an imaging configuration x-ray streak camera. Initial data with a 160-eV halfraum with Be + 0.9% Cu and polyimide ablators showed that the shock timing could be predicted to within ~ 200 ps (see Fig. 88.59).
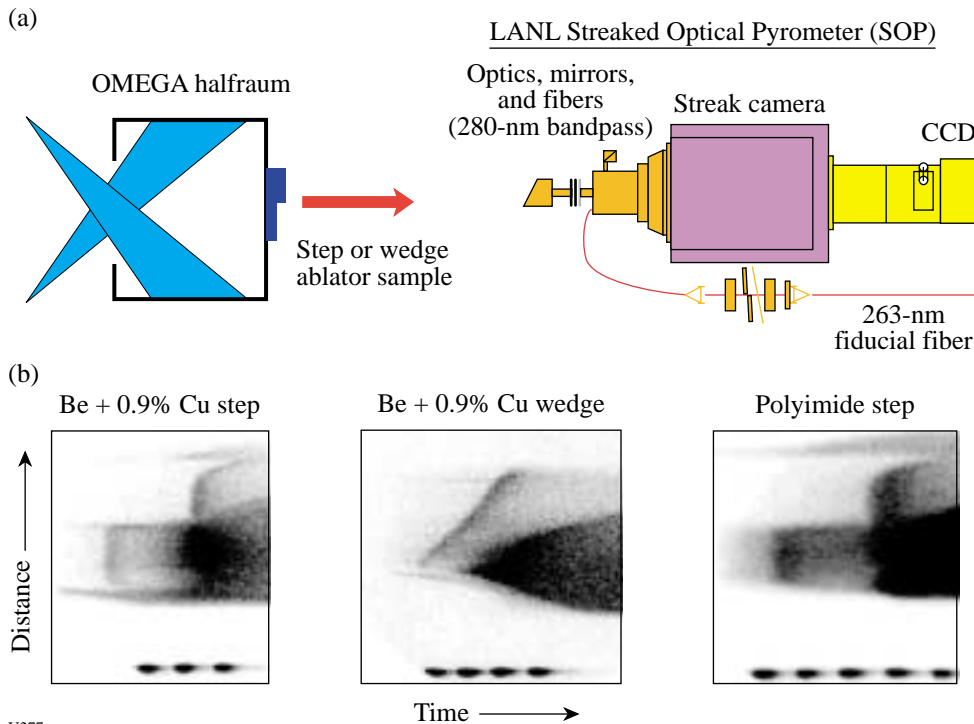
Figure 88.58
(a) Schematic of shock-timing experiments and (b) streak camera data from three configurations: Be + 0.9% Cu step; Be + 0.9% Cu wedge; and a polyimide step. The streak photographs have the time axis on the bottom (note temporal fiducial) and the space coordinate on the vertical axis.
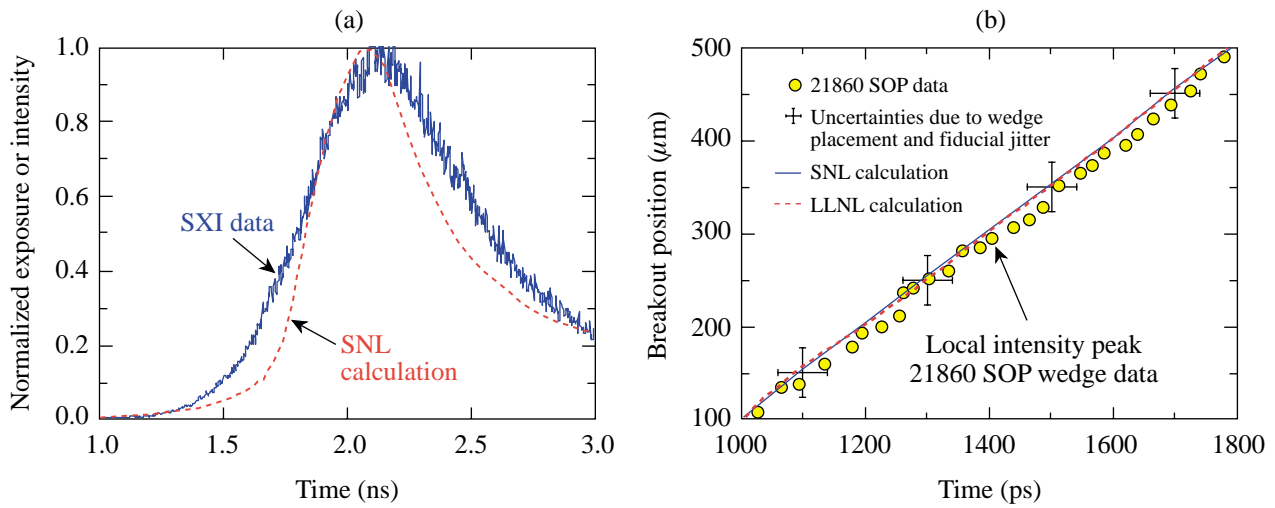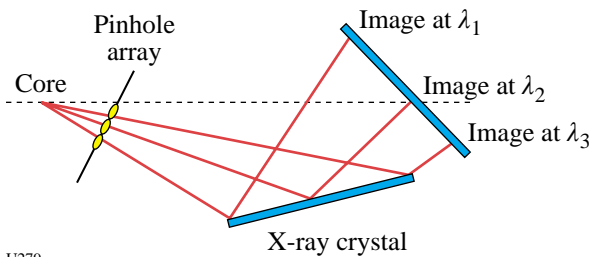
Figure 88.59

Comparison of experimental shock breakout data with SNL and LLNL calculations. (a) Ablation-front burnthrough data and comparison to SNL simulations for planar polyimide sample. (b) Shock-breakout measurements and comparison to SNL (solid line) and LLNL (dashed line) simulations for Be + 0.9% Cu wedge.

Ignition Diagnostics: A new diagnostic for measurement of the ablator areal density (ABRHOR) was tested on OMEGA. ABRHOR is designed to measure spatial variations in shell ρR and/or temperature as an indication of shell breakup and burnthrough. The technique relies on a mid-Z dopant in the ablator. Multiple monochromatic images across an x-ray energy band containing spectral features from the dopant can provide the required data. In FY01, experiments were conducted on OMEGA to test a conceptual design of this instrument based on multiple pinhole imaging off a crystal. [This is similar to an LLE-developed technique (see Fig. 88.60)]. The OMEGA test was conducted on Ti-doped CH pushers in indirect-drive implosions that were back-illuminated by the core x-ray continuum. Good data were obtained (see Fig. 88.61) from several shots with different drive and capsule parameters. The relatively poor quality of the graphite crystals used in this initial test complicated quantitative analysis. Future experiments will use a multilayer mirror to improve the quality of the data.

Figure 88.60

Schematic of ABRHOR diagnostic. Multiple monochromatic images are obtained across an x-ray energy band containing spectral features from the dopant.
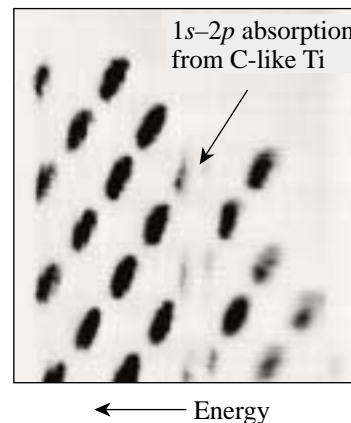
Figure 88.61

Proof-of-principle data from ABRHOR diagnostic. Multiple images of Ti-doped CH pushers are back-illuminated by the self-emission from the core continuum radiation.

IDrive: During FY01, LLNL initiated a series of experiments on OMEGA to test a new laser-driven, high-pressure source (IDrive). The new design (shown in conceptual form in Fig. 88.62) creates a plasma piston that can generate a shockless, continuously loaded high-pressure wave in a flat target. Initial efforts in July 2001 demonstrated that the concept functions as designed. Very low laser energies (less than 30 J/beam) have produced flyer velocities in excess of 12 km/s and shockless

pressure waves up to 0.5 Mbar. Figure 88.63 shows the results from some of the early experiments.

High-Z and Low-Z Equation-of-State (EOS) Experiments: During FY01, significant progress was made on EOS experiments for both high-Z and low-Z matter. Hugoniot data were obtained on diamond and water; the shock metalization thresholds were identified for water, diamond, LiF, and sap-
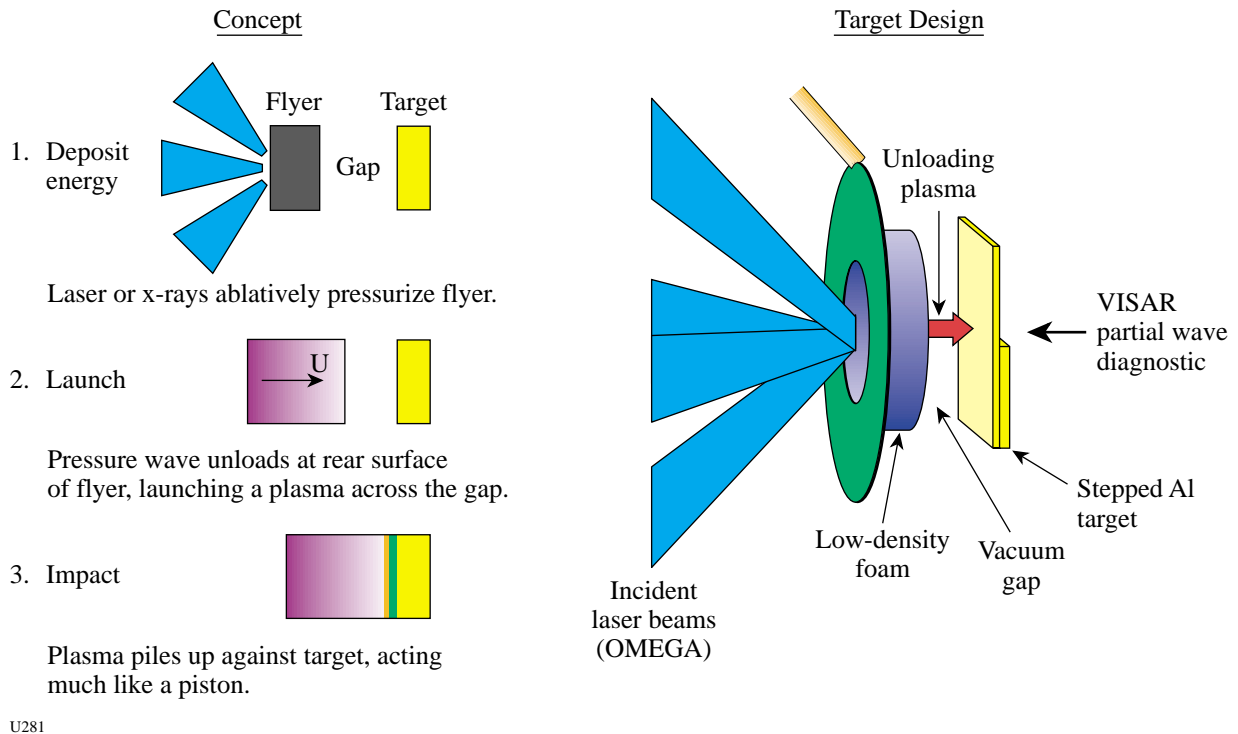

Figure 88.62
Schematic illustrating the IDrive shockless drive technique and a sketch of the target design for the IDrive experiments.
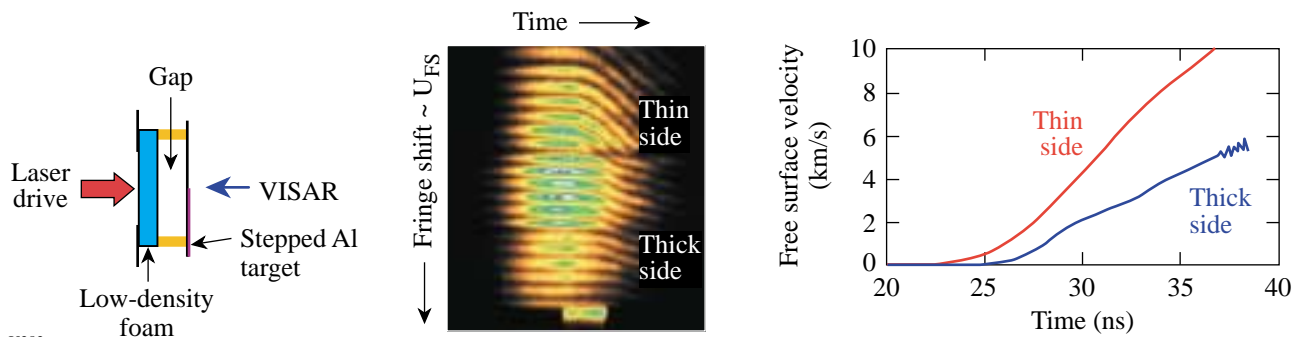

Figure 88.63
Initial results from the IDrive experiments show the presence of a shockless pressure wave in aluminum.

phire; the shock-melting transition in diamond was accurately identified; accurate double-shock experiments were carried out on water using the transparent anvil technique; and initial experiments were carried out to determine shock-induced melting in metals. In addition, the ASBO diagnostic system (the workhorse of EOS experiments) was upgraded to dual-VISAR capability.

Direct-Drive Richtmeyer–Meshkov (RM) Instability Experiments: In FY01 a series of direct-drive RM experiments were carried out on planar targets with initial perturbation amplitudes of 22 μm and 7 μm and a perturbation wavelength of

150 μm. The experimental data were compared (see Fig. 88.64) with simulations using linear (Meyer–Blewitt) and nonlinear (Sadot) models that do not include shock proximity. In both cases, the models over-predicted the amplitude growth.

Supersonic Jet Experiments: Collaborative experiments among AWE (United Kingdom), LANL, and LLNL continued to investigate the interaction of a supersonic jet with a counter-propagating shock. During FY01, these experiments provided high-quality benchmark data for comparison to the CAL (LLNL), RAGE (LANL), and NYM-PETRA (AWE) hydrocodes (see Fig. 88.65).
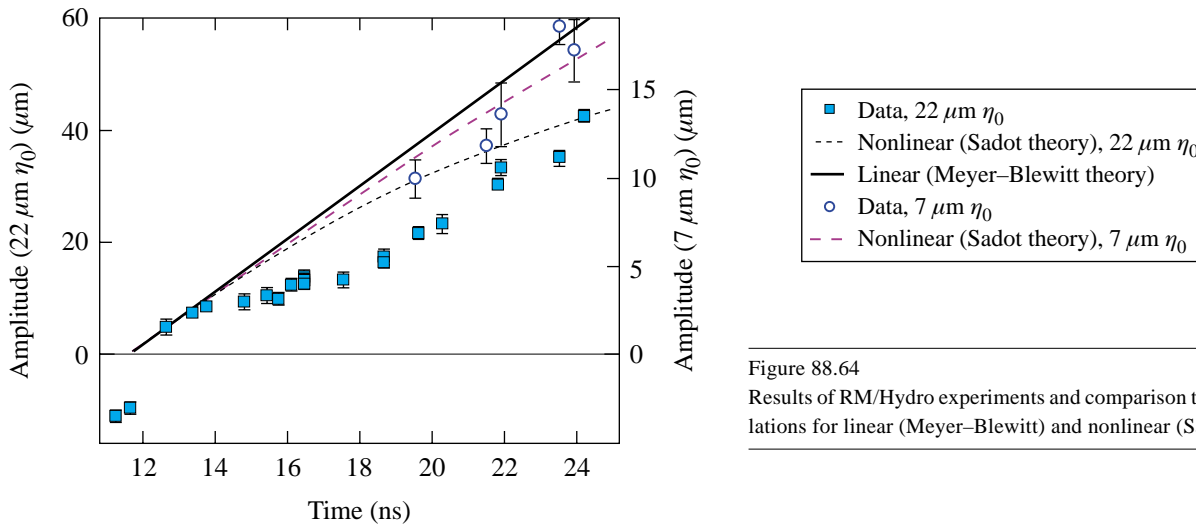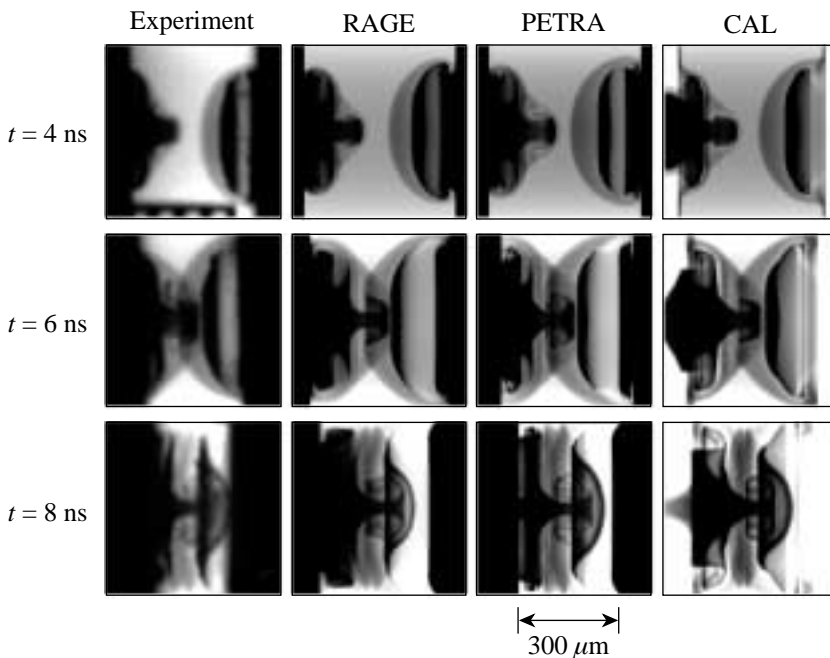

U283

Figure 88.64

Results of RM/Hydro experiments and comparison to theoretical calculations for linear (Meyer–Blewitt) and nonlinear (Sadot) theories.

U284

Figure 88.65

Comparison of supersonic jet experiments with various multidimensional computer simulations. The jet and shock are generated in two opposed halfraums. The images are created by x-ray backlighting of the interaction region.

Nonideal Backlit Implosions (NIBI): During FY01, experiments were initiated to investigate the effects of nonuniform illumination on direct-drive capsule implosions. A subset of OMEGA beams was used to implode a capsule while the remaining beams were used to produce x rays from a Fe target to backlight the imploding target. Figure 88.66 shows the results from a near-uniform illumination experiment (shot 23543) and from an implosion with imposed asymmetry in the capsule irradiation (shot 23544).
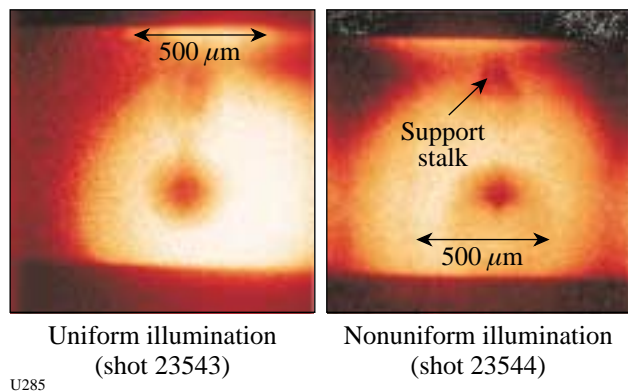
Figure 88.66

X-ray backlit images (Fe backlighter) from near-symmetric (shot 23543) and nonuniform illumination (shot 23544) of low-convergence implosions.

Slit Closure: One of the capability development programs carried out in FY01 involved the investigation of slit and pinhole closure by soft x rays. Figure 88.67 shows the experimental configuration and data obtained on two of these experiments. In this case, a Ti backlighter foil was irradiated by some of the OMEGA beams, and the transmission of the resulting x rays through a slit was measured with a streak camera. The graph compares the x-ray transmission through the slit as a function of time when a Be foil is placed between the Ti foil and the pinhole and when no foil is used. The Be foil is designed to block soft x rays from the Ti from irradiating the pinhole. No difference in transmission between these two cases is observed, implying that soft x rays are not the predominant mechanism for inducing slit or pinhole closure in such configurations. Future shots will investigate the effect of slit tamping on the closure.

Gas-Filled Sources: Experiments continued under the NWET program to develop the efficient x-ray sources to be used as
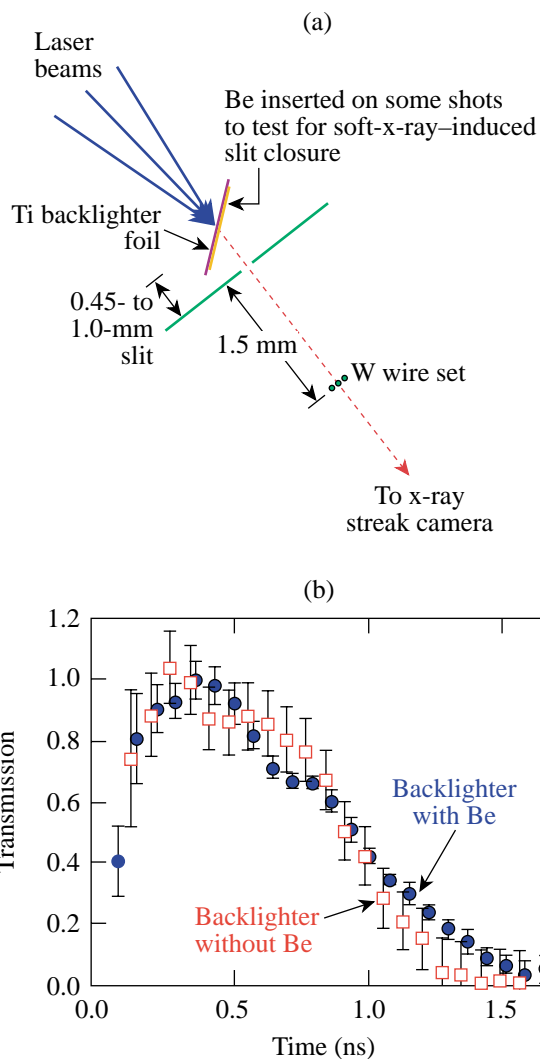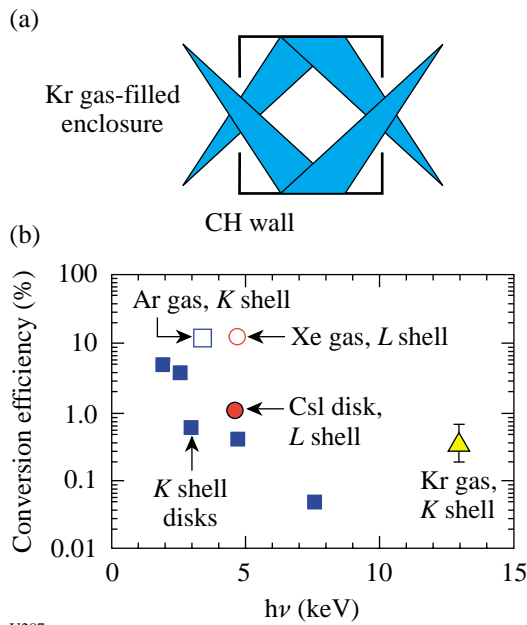
Figure 88.67

(a) Schematic of slit closure experiment and (b) results of transmission measurements.

backlighters for high-ρR and high-Z applications. During FY01, Kr K-shell emission was added to the list of efficient underdense multi-keV emitters. The experimental configuration (a Kr-filled CH cylinder) and a summary of the x-ray conversion results for emitters with energy in the range of 2 to 13 keV are shown in Fig. 88.68. The latest Kr gas experiments produced ~0.3% conversion in the ~13-keV Kr K-shell emission.

(a)

Kr gas-filled enclosure

CH wall

(b)

Figure 88.68
(a) Schematic of gas-filled can radiation source experiments. (b) Results of conversion efficiency measurements for a series of gases and disks.

2. Los Alamos National Laboratory Campaigns

In FY01 LANL performed five campaigns on OMEGA. This work has been documented in the form of pre- and postshot reports:

a. LANL ID01-1: Double shells in cylindrical hohlraums and ACE-A and ACE-B
   – Preshot report LA-UR-00-5574
   – Double-shell postshot report LA-UR-01-0432

– ACE-A postshot report LA-UR-01-1426
– ACE-B postshot report LA-UR-01-5433

b. DDCYL 01-1: Direct-drive cylinders
   – Preshot report LA-UR-01-0953
   – DDCYL postshot report LA-UR-01-5511

c. LANL ID01-2: X-ray backlighter development and ACE
   – Preshot report LA-UR-01-1659
   – ACE-A postshot report LA-UR-01-5559

d. LANL ID01-3: High-yield nuclear diagnostic development and ACE
   – Preshot report LA-UR-01-4381
   – ACE-A postshot report LA-UR-01-5560
   – High-yield postshot report
   – Direct-drive double shells (DDCYL 01-2 cancelled because of the 9/11 events)
   – Preshot report LA-UR-01-5202

Double-Shell Capsules: Work continued on double-shell capsules as an alternative for ignition on the NIF. Previously, good results (high measured neutron yield relative to 1-D clean calculations) had been obtained in spherical hohlraums (a.k.a. "tetrahedral hohlraums," referring to the locations of the laser entrance holes) with excellent irradiation symmetry. Representative capsules were shot on OMEGA to confirm that similar good results could be obtained with NIF-relevant symmetry in cylindrical hohlraums. Good results were obtained with deuterium-filled capsules, showing that drive symmetry was not the principal issue of performance for these capsules (see Fig. 88.69). Subsequently, larger capsules were shot using direct-drive illumination that would remove any
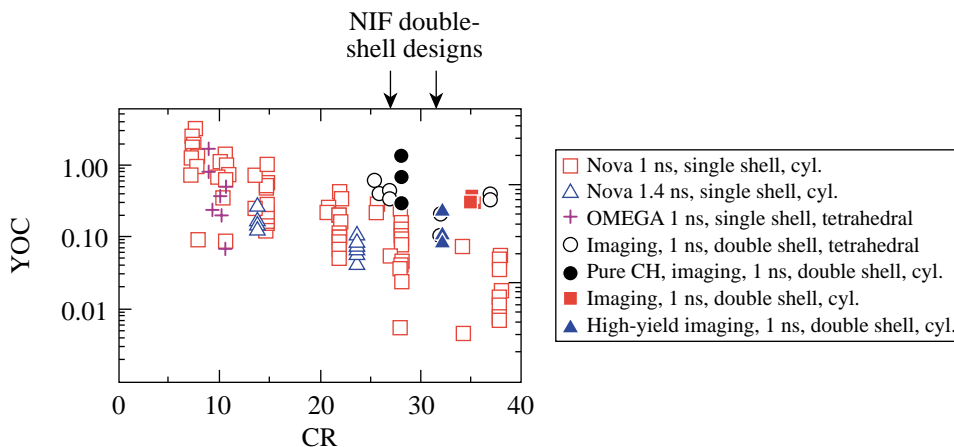
Figure 88.69
Measured neutron yield divided by 1-D, clean calculated yield (YOC) versus convergence ratio (CR) for all OMEGA imaging and pure-CH imaging shots to date, in tetrahedral and NIF-style cylindrical hohlraums. The data for the NIF-style hohlraums is shown as solid points, while the tetrahedral results are shown as circles or open crosses. In the legend, "cyl" is a cylindrical hohlraum.

M-band asymmetries due to laser spots in the hohlraums. Poor results were obtained in this series. The issues of target fabrication, mix, and direct-drive physics are being investigated to understand the later results.

X-Ray Backlighting Sources: The development of x-ray backlighting sources and the optimization of x-ray conversion efficiency for these sources are important for the design of future NIF experiments. Various mid-*Z* elements and a variety of spot sizes and intensities of 3ω light have been investigated on OMEGA experiments. Data showing the dependence of conversion efficiency on spot size at similar irradiance have been obtained (Fig. 88.70). The peak x-ray conversion as a function of intensity has been identified for different configurations.

ACE Experiments: The ACE experiments successfully obtained data for the high-energy-density support of the Stockpile Systems Program. Some experiments featured an innovative backlighter system that provides very bright emission and is flat in intensity across the field of view (illustrated in Fig. 88.71).

Direct-Drive Cylindrical Implosions: Direct-drive cylinder work continued in two campaigns. The ablative RT work evaluated target fabrication and image quality to achieve quantitative data for comparison to hydrocode predictions. Figure 88.72 shows imaging x-ray streak camera data from such a cylindrical implosion with a ramp drive pulse. Just before the end of the 2.5-ns linear ramp, the chlorine in the
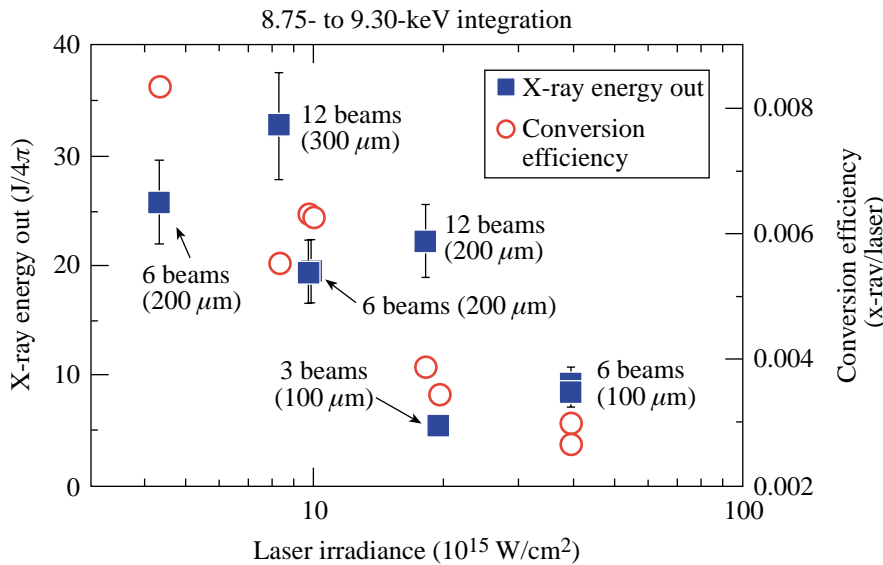

Figure 88.70
Plot of measured x-ray energy in He-α lines of Zn taken using a time-integrated Henway spectrometer versus laser irradiance from overlapped beams with indicated spot size.

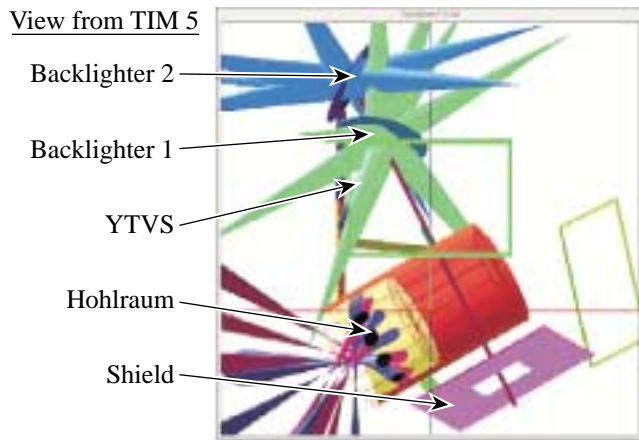Figure 88.71
The ACE-B geometry with two backlighters irradiated by 17 beams to carry out radiography of a halfraum with 12 drive beams.

marker layer burns through due to the formation of spikes by the action of the RT instability. Unfortunately, it has been decided that, at present, targets with sufficiently small and controlled surface roughness cannot be fabricated to quantitatively address the relevant physics of this experiment so this campaign has been stopped. The direct-drive cylinder mix program has made significant success in demonstrating measurable mix in a convergent, compressible plasma experiment. Thick (60- to 73-μm) ablators separate the direct-drive laser absorption region from the "pure" hydrodynamic marker. Detailed calculations are being made to model this data using a number of codes, including the *RAGE* adaptive mesh refinement code at Los Alamos illustrated in Fig. 88.73. This year mix-width data (Fig. 88.74) were taken at different times during the implosion and compared to the *RAGE* simulations.

NIF Diagnostics: Los Alamos continues to develop Phase 2 fusion product diagnostics for the NIF, including both the Gas Cerenkov gamma-ray burn history diagnostic and pinhole-aperture neutron imaging. The Gas Cerenkov System obtained definite evidence for the DT fusion gamma on OMEGA. The neutron imaging system, in collaboration with CEA and LLE, obtained images for the first time.
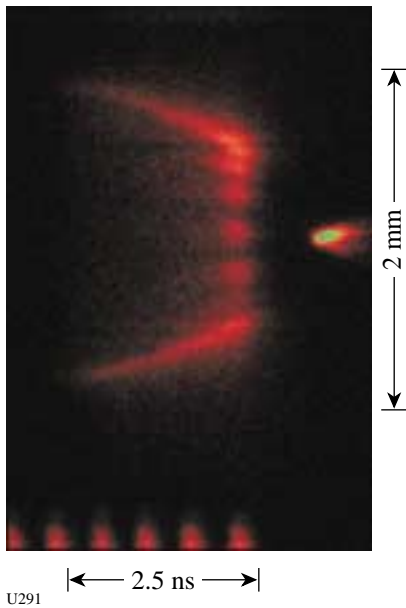

U292

Figure 88.73
RAGE simulation of the volume fraction of a gold marker in an *r-θ* calculation at 3.0 ns into a direct-drive cylindrical mix implosion.

U291

Figure 88.72
Imaging x-ray streak camera (IXRSC) image from shot 22622 showing intensity transversely across the cylinder (up–down) versus time (left–right). The ablation surface implodes, with the spikes of the original $m = 14$ perturbation burning through just before the end of the 2.5-ns linear ramp laser drive. Subsequently, the core of the cylinder implodes and lights up in self-emission.
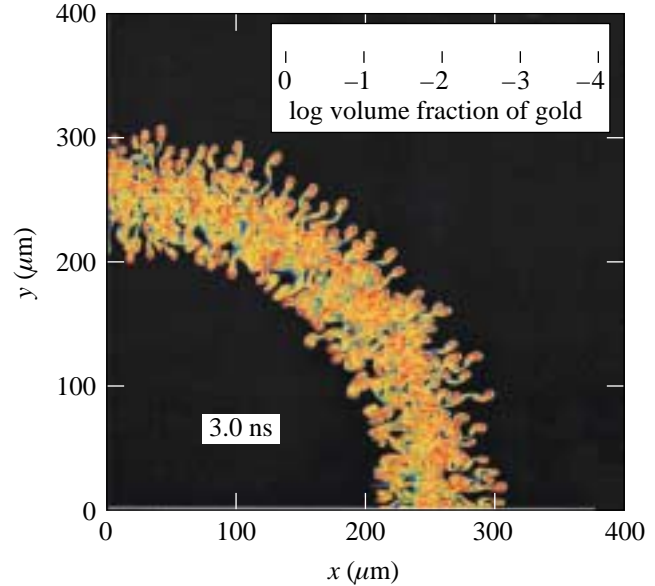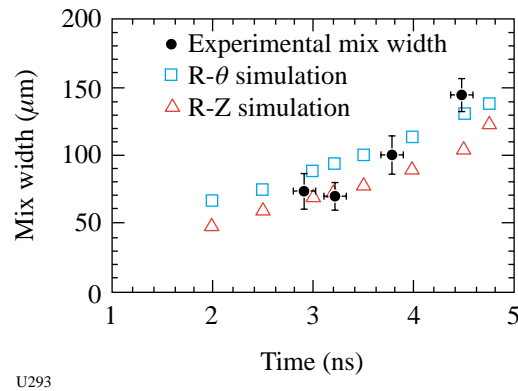

U293

Figure 88.74
Comparison of experimental measurements of rough gold marker mix width in time with *RAGE* simulations.

3. CEA Experiments

CEA scientists participated in several OMEGA experiments during FY01 including neutron imaging development and evaluation and measurement of gamma yields on OMEGA.

Imaging of the neutrons produced by implosions on the NIF and the LMJ will require spatial resolution as great as 5 μm to distinguish failure mechanisms such as poor implosion symmetry or improper laser pulse shaping. Coded imaging, either by penumbral or annular aperture, will be used to achieve high resolution and good sensitivity.[2] In FY00, CEA implemented a neutron imaging system (NIS) on OMEGA based on penumbral imaging using a biconical aperture. Using NIS, the neutron burn regions of imploded DT-filled glass microballons with 2.5- and 4.2-μm-thick walls were imaged and produced images with FWHM's of 78 and 62 μm, recorded with a resolution of 60 and 45 μm, respectively.[3]

This year (FY01), a spatial resolution of 20 μm was attained on implosions of CH and glass targets. The smallest features observed on the implosion of 15-atm-DT-filled CH capsule implosions were ~30 μm.

To improve the NIS resolution, LLE drilled a hole in the concrete floor of the Target Bay, allowing a 13-m line of sight and a 1.6-m concrete shield for the NIS CCD detector (Fig. 88.75).

In parallel, a new neutron detector with 250-μm pixels was installed. This detector is made by filling an array of 160,000 capillaries[4] with a high-optical-index liquid scintillator. The optical-index step between the glass (1.49) and the liquid (1.58) traps the scintillation light produced by the slowing down of the recoil protons scattered by the 14-MeV neutrons. Both the pixel size and the transverse range of the recoil protons limit the neutron detector's spatial resolution to 1.1 mm. With a biconical aperture with a 200-μm field of view placed at 160 mm from target center, the ultimate resolution of NIS is now 17-μm FWHM.

Direct-drive implosions of DT-filled glass targets and CH targets were conducted during the experimental campaign. A typical unfolded neutron image from a CH target implosion (shot 23445) is shown in Fig. 88.76. The target in this case was a 932-μm-diam, 18.9-μm-thick CH shell filled with 15 atm of DT and produced a yield of 2×10^{13}.
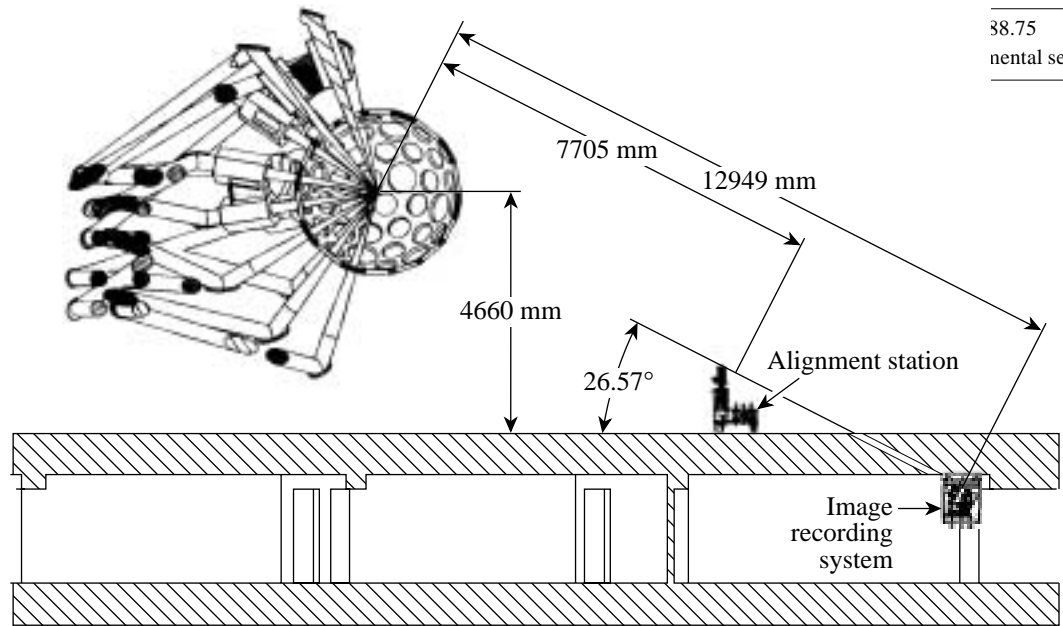
88.75
...nental setup of the neutron imaging system.

7705 mm

12949 mm

4660 mm

26.57°

Alignment station

Image recording system

U294

A new neutron detector is now being constructed. The scintillator will be loaded with deuterium to reduce the range of the recoil protons. The expected resolution of the new **detector** will be less than 0.5 mm. In parallel with the construction of the new detector, a thin annular aperture is under development. The first attempt will be made with a 5-cm-thick, 0.66-mm-diam cylinder of tungsten. This effort should lead to high-resolution neutron imaging at a low (~10^{12}) level of neutron production.

REFERENCES

1. C. A. Iglesias and S. J. Rose, Astrophys. J. Lett. **466**, L115 (1996); F. J. Rogers, B. G. Wilson, and C. A. Iglesias, Phys. Rev. A, Gen. Phys. **38**, 5007 (1988).

2. R. A. Lerche *et al.*, Laser Part. Beams **9**, 99 (1991).

3. L. Disdier, A. Rouyer, A. Fedotoff, V. Yu. Glebov, C. Stoeckl, and F. J. Marshall, "Neutron Prenumbral Imaging at OMEGA," submitted to Nuclear Instruments & Methods in Physics Research, Section A; Laboratory for Laser Energetics LLE Review **86**, 74, NTIS document No. DOE/SF/19460-393 (2001). Copies may be obtained from the National Technical Information Service, Springfield, VA 22161.

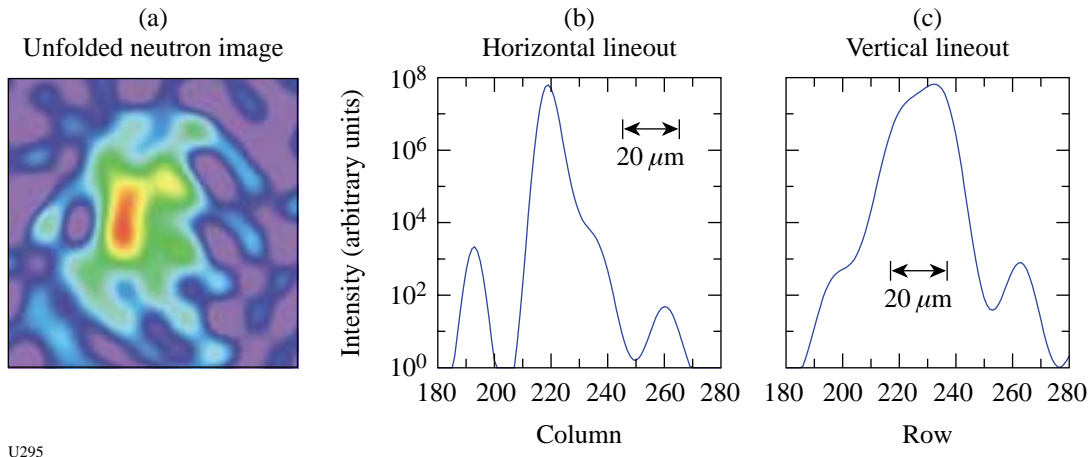4. P. Annis *et al.*, Nucl. Instrum. Methods Phys. Res. A **367**, 377 (1995).

Figure 88.76

(a) Neutron image (200×200 μm^2) on shot 23445; (b) horizontal and (c) vertical profiles (43-μm and 75-μm FWHM, respectively). The arrows represent 20 μm in the target plane.